Chapter: 5

Field Induced Phase Transition in MPB Region of (1-x)$Bi(Mg_{3/4}W_{1/4})O_3$-x$PbTiO_3$ Ceramics

5.1 Introduction

Ferroelectric and piezoelectric ceramics are subjected to external electric field during operation for various applications. Since the crystal structure is non-centrosymmetric, the magnitude of polarization and electric field response of these ceramics strongly depends upon the crystal structure. In polycrystalline ferroelectric ceramics, one does not observe the piezoelectricity because of the random orientation of stress induced polarization or electric field induced strain, that cancel out each other with net response at microscopic level to be zero. To observe piezoelectricity in ceramic samples, the ferroelectric ceramics are subjected to high dc-electric field poling that imparts a polar axis in polycrystalline samples due to remnance of polarization in the externally applied field direction [Jaffe et al 1972]. Thus it is essential to understand the effect of externally applied electric field on the crystal structure of MPB ceramics. In recent years, it is now established that the electric field poling of ferroelectric ceramics around the MPB compositions significantly modifies the crystal structure and changes the crystallographic phase stabilities. Electric field induced structural changes has been investigated in several MPB systems such as $PbZr_{1-x}Ti_xO_3$ [Schönau et al. (2007), Guo, et al. (2000)], $(1-x)Pb(Mg_{1\backslash3}Nb_{2\backslash3})O_3$-$xPbTiO_3$ [Park et al. (1997), [Bokov et al. (2008), Guo et al. (2002)], $0.67Pb(Mg_{1/3}Nb_{2/3})O_3$-$0.33PbTiO_3$ [Zheng et al. (2015)], $0.68Pb(Mg_{1/3}Nb_{2/3})O_3$-$0.32PbTiO_3$ [PMN-0.32PT] [Li et al. (2008)], $(1-x)Pb(Zn_{1\backslash3}Nb_{2\backslash3})O_3$-$xPbTiO_3$ [Uchino et al. (2000); Noheda et al. (2001)], (Pb, La)(Zr, Sn,Ti)O_3 [Gao et al. (2015)] $(1-x)Bi(Ni_{1/2}Ti_{1/2})O_3$-$xPbTiO_3$ [Pandey and Singh (2014)], $(1-x)Bi(Mg_{1/2}Ti_{1/2})O_3$-$xPbTiO_3$ [Upadhyay and Singh (2016)], $(1-x)Bi(Mg_{1/2}Zr_{1/2})O_3$-$xPbTiO_3$ [Upadhyay et al. (2017)] etc.

Effect of electric field poling on the crystal structure of (1-x)Bi($Mg_{3/4}W_{1/4}$)O_3-x$PbTiO_3$ ceramics has not been investigated yet by earlier researchers. In this chapter, we present the result of structural characterizations on the electric field poled samples at various electric field strength. We have selected some representative compositions of (1-x)Bi($Mg_{3/4}W_{1/4}$)O_3-x$PbTiO_3$ ceramics across MPB to understand the effect of poling field on the crystal structure.

5.2 Experimental Details

(1-x)Bi($Mg_{3/4}W_{1/4}$)O_3-x$PbTiO_3$ ceramic samples with compositions x = 0.61, 0.62, 0.63 and 0.67 were selected for the electric field induced structural characterizations. The samples were prepared by the solid state ceramic method as described in Chapter 2. For electric field poling at various strengths, sintered pellets of different compositions were electroded using fired-on silver paste. The electroded pellets were poled at 120°C temperature in silicon oil at different electric fields (E) viz. 10, 20, 30 and 40 kV. For recording the XRD pattern of the poled samples, the silver electrode was removed. The XRD patterns of unpoled and poled pellets of (1-x)BMW-xPT were recorded at scan rate of 1° per minute on 0.02° scan step in the 2θ range 10°-100°. The FullProf Suite was used for Le-Bail profile matching structural analysis of the XRD data of unpoled and poled samples [Carvajal et al. (2011)]. Due to domain evolution the preferred orientation can leads to intensity mismatch of calculated and observed pattern of XRD data in the Rietveld fitting. Therefore profile matching analysis was carried out by Le-Bail refinement, which helps in overcoming of preferred orientation during structural analysis.

5.3 Results and Discussion

The Powder x-ray diffraction (XRD) patterns of unpoled (1-x)BMW-xPT polycrystalline piezoceramic with compositions x = 0.61, 0.62, 0.63 and 0.67 in the 2θ

range 10°-100° is shown in **Fig. 5.1**. The inset in **Fig. 5.1** shows the zoomed (111) superlattice peak, appearing due to ordering of B-site cations. Detailed structural characterization of virgin (1-x)BMW-xPT samples is already discussed in Chapter 3. The compositions with x = 0.63 and 0.67 are predominantly tetragonal with *I*4/*m* space group. The compositions with x = 0.61 and 0.62 have coexistence of tetragonal (I4/m) and cubic (*Fm*-3*m*) structures. As can be seen from inset to **Fig. 5.1**, the superlattice peak due to B-site cationic ordering is present in all the compositions. We shall discuss now the effect of electric field poling on the crystal structure of these compositions.

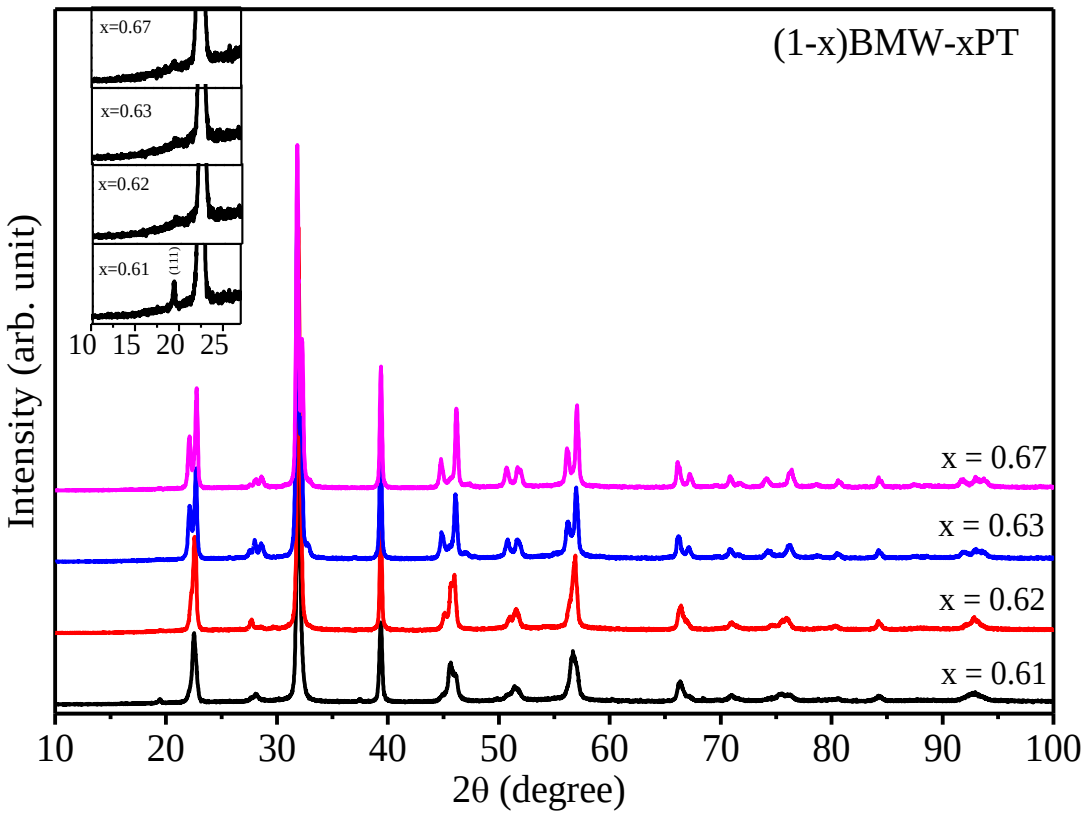

Figure 5.1 Powder XRD patterns of (1-x)Bi($Mg_{3/4}W_{1/4}$)O_3-x$PbTiO_3$ piezoceramics with compositions x = 0.61, 0.63 and 0.67 in the 2θ range of 10°- 100°. The inset shows the zoomed (111) superlattice reflection appearing due to B-site cationic ordering.

5.3.1 Crystal Structure of Electric Field Poled 0.39BMW-0.61PT Ceramic

The evolution of some selected pseudocubic (110), (111) and (200) XRD peak profiles for the 0.39BMW-0.61PT ceramic pellet samples poled at electric fields 10, 20, 30 and 40 kV/cm along with that of un-poled sample are shown in **Fig. 5.2**. The crystal structure of the unpoled sample with x = 0.61 is the coexistence of ordered cubic and ordered tetragonal phases which results into a triplet for the (200) pseudocubic profile. As can be seen from **Fig. 5.2**, the (200) XRD profiles for the electric field poled samples are clearly different from that for the unpoled sample. This suggests that there is definitely some structural change in the 0.39BMW-0.61PT ceramic after electric field poling. After electric field poling the (200) pseudocubic XRD profile appear as doublet for all field strength. Thus the coexisting cubic structure is transforming into tetragonal structure after electric field poling. The (111) pseudocubic profile remain as a single for poled as well as unpoled 0.39BMW-0.61PT samples. The (110) profile also does not show any significant change as the splitting in this peak is not resolved due to large broadening and asymmetry. To confirm this crystallographic modification further, we performed full pattern profile matching analysis of the XRD patterns of the poled samples. Rietveld structural analysis confirms that the coexisting cubic and tetragonal structures of 0.39BMW-0.61PT converted into tetragonal structure after electric field poling. Further, the superlattice peak around 19^{o} due to B-site cationic ordering disappears after poling making the structure to be disordered tetragonal phase with space group *P*4*mm* [see **Fig. 5.6**]. The full pattern fit of the XRD data using Le-Bail profile matching analysis with tetragonal P4mm space group, for samples poled at 30 kV/cm, of three representative compositions, is shown in **Fig. 5.6**. The fit is quite good confirming the transformation of structure into disordered tetragonal phase for poled samples of all the three compositions.

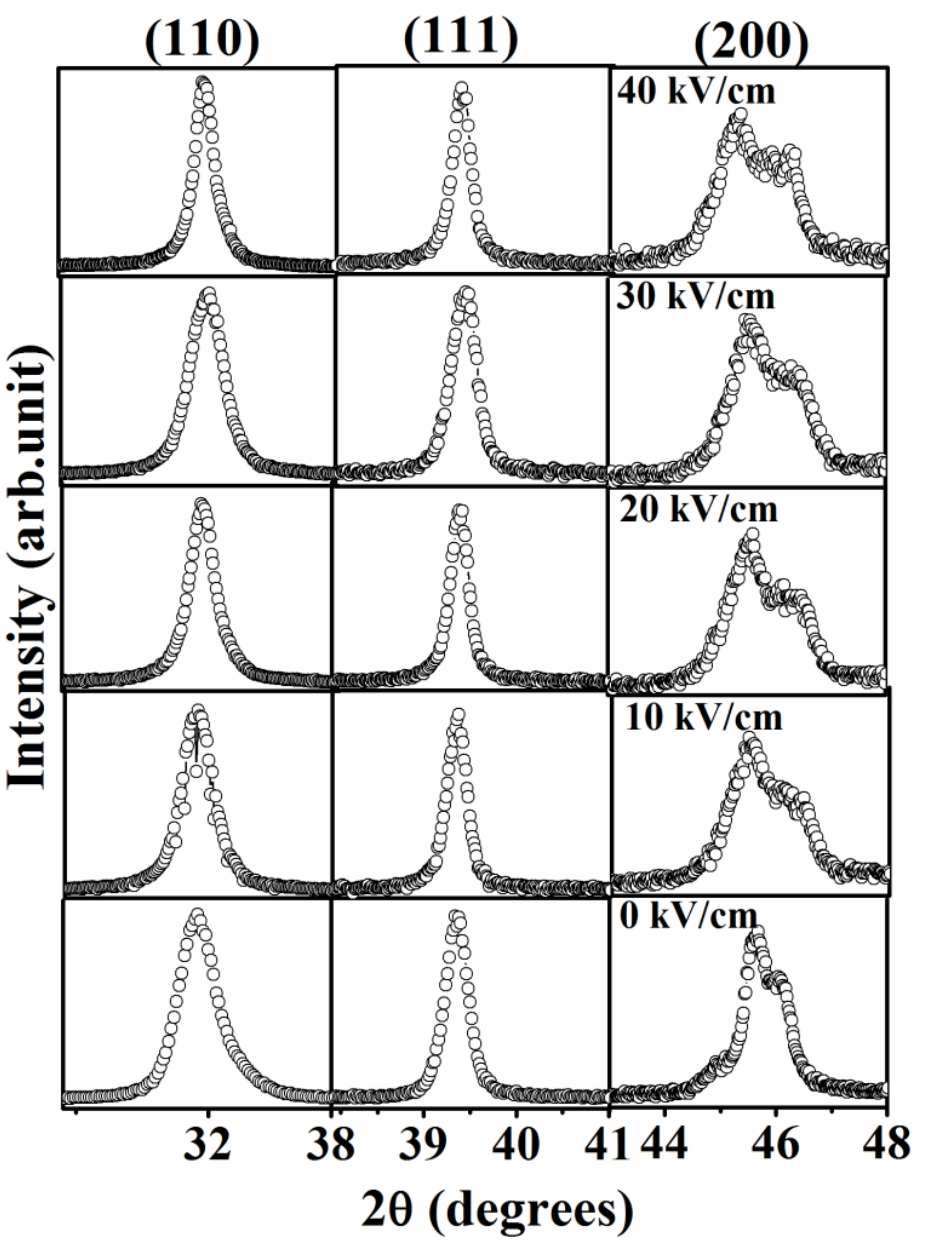

Figure 5.2 Evolution of the pseudocubic (110), (111) and (200) XRD profiles of 0.39BMW- 0.61PT pellets poled at different poling field strength.

5.3.2 Crystal Structure of Electric Field Poled 0.38BMW-0.62PT Ceramic

Similar to the 0.39BMW-0.61PT, the crystal structure of virgin sample of 0.38BMW-0.62PT is also coexistence of ordered cubic (*Fm*-3*m*) and ordered tetragonal (*I*4/*m*) phases. After electric filed poling a similar kind of crystallographic modifications has been observed for this composition also. The selected pseudocubic

XRD (110), (111) and (200) peak profiles for x = 0.62 poled at different field strength such as 30 and 40 kV/cm along with that for the unpoled sample are shown in **Fig. 5.3**. As can be seen from **Fig, 5.3**, for unpoled sample, the phase coexistence is revealed by the triplet peaks of the (200) profiles while it becomes doublet after electric field poling. The full pattern Le-Bail profile matching analysis confirms that the crystallographic structural evolution of 0.38BMW-0.62PT after electric field poling is similar to that in the 0.39BMW-0.61PT.

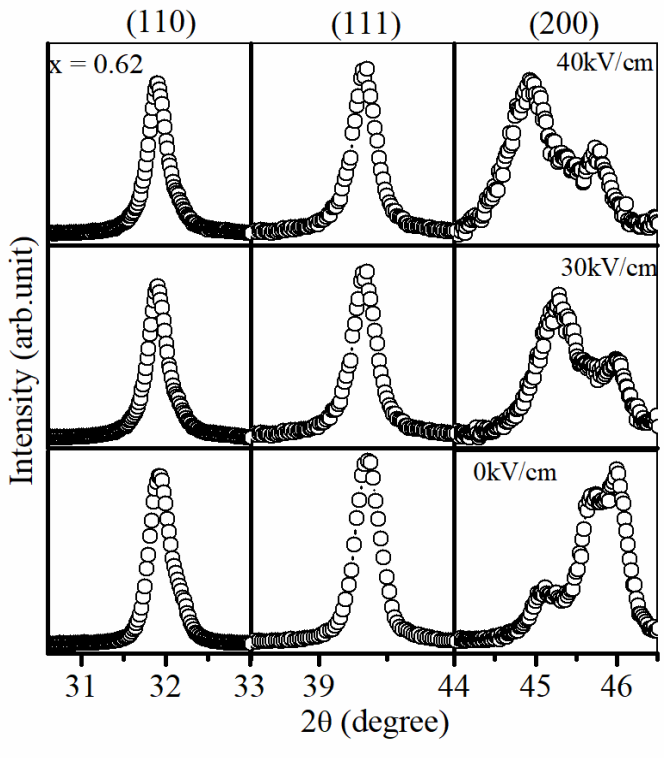

Figure 5.3 Evolution of the pseudocubic (110), (111) and (200) XRD profiles of 0.38BMW-0.62PT pellets poled at different poling field strength.

5.3.3 Crystal Structure of Electric Field Poled 0.33BMW-0.67PT Ceramic

The selected pseudocubic (110), (111) and (200) XRD peak profiles for the composition x = 0.67 poled at different electric fields 10, 20 and 30 kV/cm along with unpoled sample are shown in **Fig. 5.4**. As discussed in Chapter 3, the crystal structure

of virgin sample for x = 0.67 is predominantly B-site ordered tetragonal with space group *I*4/*m*. There is small fraction of cubic phase as evidenced from the slightly lifted portion of the background in between the (002)/(200) doublet of the tetragonal phase. After electric field poling with strength 20kV/cm and higher, the structure becomes completely tetragonal as the coexisting cubic phase gets eliminated. In addition, the intensity of the tetragonal (002) peak increases significantly while that of (200) peak decreases. This is attributed to the domain reorientation along c-axis direction due to electric field poling. Similar domain reorientation along c-axis direction has been reported in tetragonal compositions of other B-based MPB ceramics also such as (1-x)Bi($Ni_{1/2}Zr_{1/2}$)O_3-x$PbTiO_3$ [Pandey and Singh (2014)], (1-x)Bi($Mg_{1/2}Ti_{1/2}$)O_3-x$PbTiO_3$ [Upadhyay and Singh (2016)], (1-x)Bi($Mg_{1/2}Zr_{1/2}$)O_3-x$PbTiO_3$ [Upadhyay et al. (2017)]. The superlattice reflection due to B-site cationic ordering is found to be absent in the electric field poled samples. This suggests that ordered tetragonal structure transforms into disordered tetragonal structure during electric field poling. Temperature dependent order-disorder transition is known in several crystallographically ordered structures such as beta phase of brass. Since poling of the samples is done at 120^{o}C, application of the electric field of higher strength is providing sufficient activation energy for the migration of B-site cations resulting into disordered structures. The Le-Bail full pattern profile matching analysis using tetragonal structure (space group *P*4*mm*) of sample poled at different electric field have been carried out which confirms the tetragonal structure. The Le-Bail full pattern profile matching analysis fit using tetragonal structure (space group *P*4*mm*) for sample poled at 30 kV/cm is shown in **Fig. 5.6**, which is quite good.

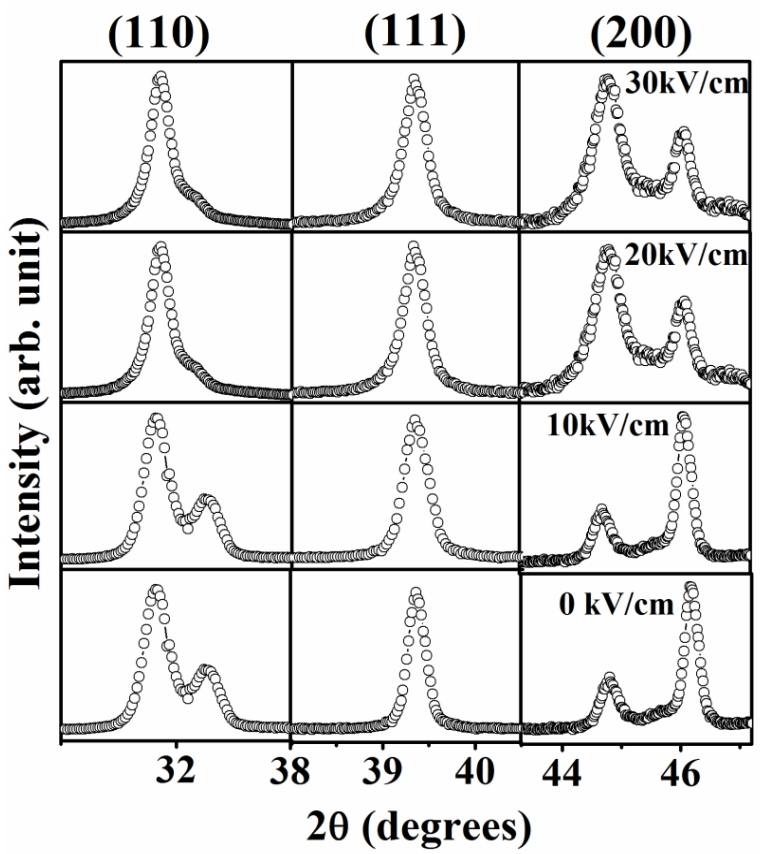

Figure 5.4 Evolution of the pseudocubic (110), (111) and (200) XRD profiles of 0.33BMW- 0.67PT pellets poled at different poling field strength.

5.3.4 Crystal Structure of Electric Field Poled 0.37BMW-0.63PT Ceramic

The selected pseudocubic (110), (111) and (200) XRD peak profiles for 0.37BMW-0.63PT poled at different electric field strength such as 10, 20, 30 and 40 kV/cm along with the unpoled sample are shown in **Fig. 5.5**. Since the crystal structure of 0.37BMW-0.63PT is predominantly tetragonal similar to 0.33BMW-0.67PT, the electric field induced structural modifications to this composition is also similar. However, as the composition with x = 0.63 is more close to MPB, the domain reorientation along c-axis for this composition is observed even at lower electric field (10 kV/cm) than that for the composition with x = 0.67 (E = 20 kV/cm or more). The full pattern Le-Bail profile matching analysis confirms the disordered tetragonal

structure with space group *P*4*mm* for the poled samples of 0.37BMW-0.63PT also. The full pattern Le-Bail profile matching fit for the sample poled at 30 kV/cm is shown in **Fig. 5.6** which is quite satisfactory.

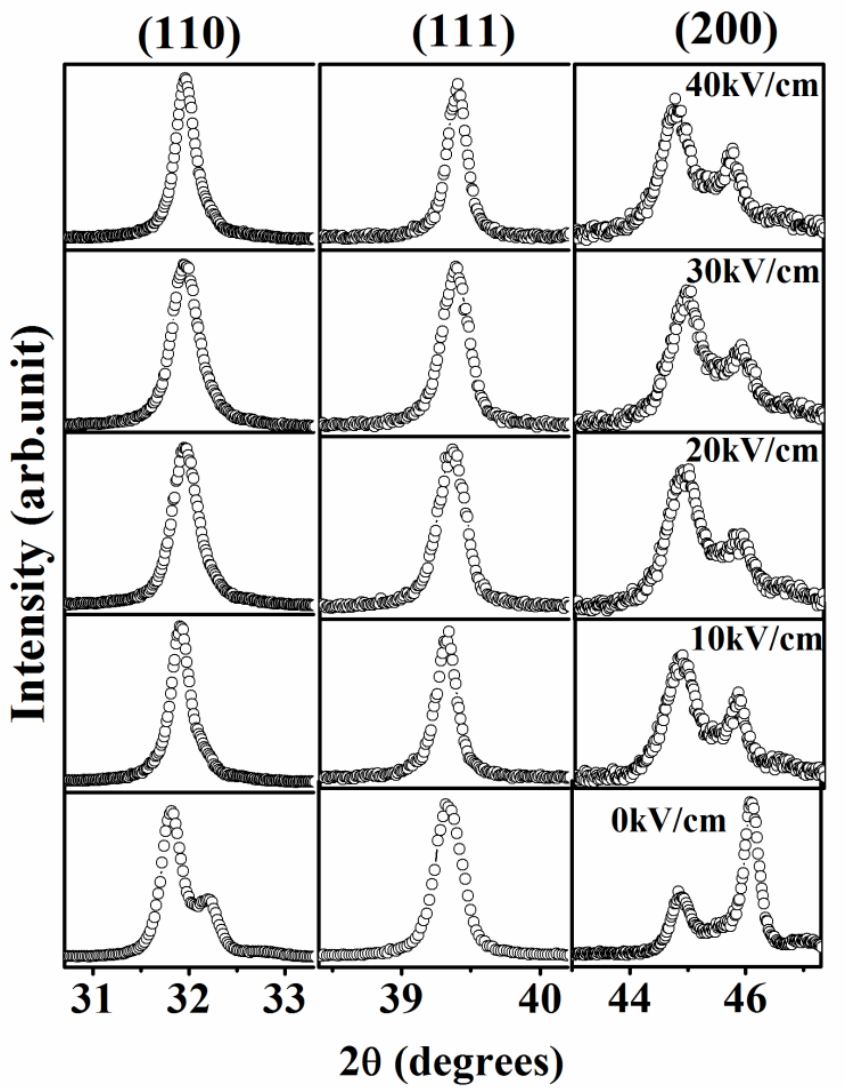

Figure 5.5 Evolution of the pseudocubic (110), (111) and (200) XRD profiles of 0.37BMW-0.63PT pellets poled at different poling field strength.

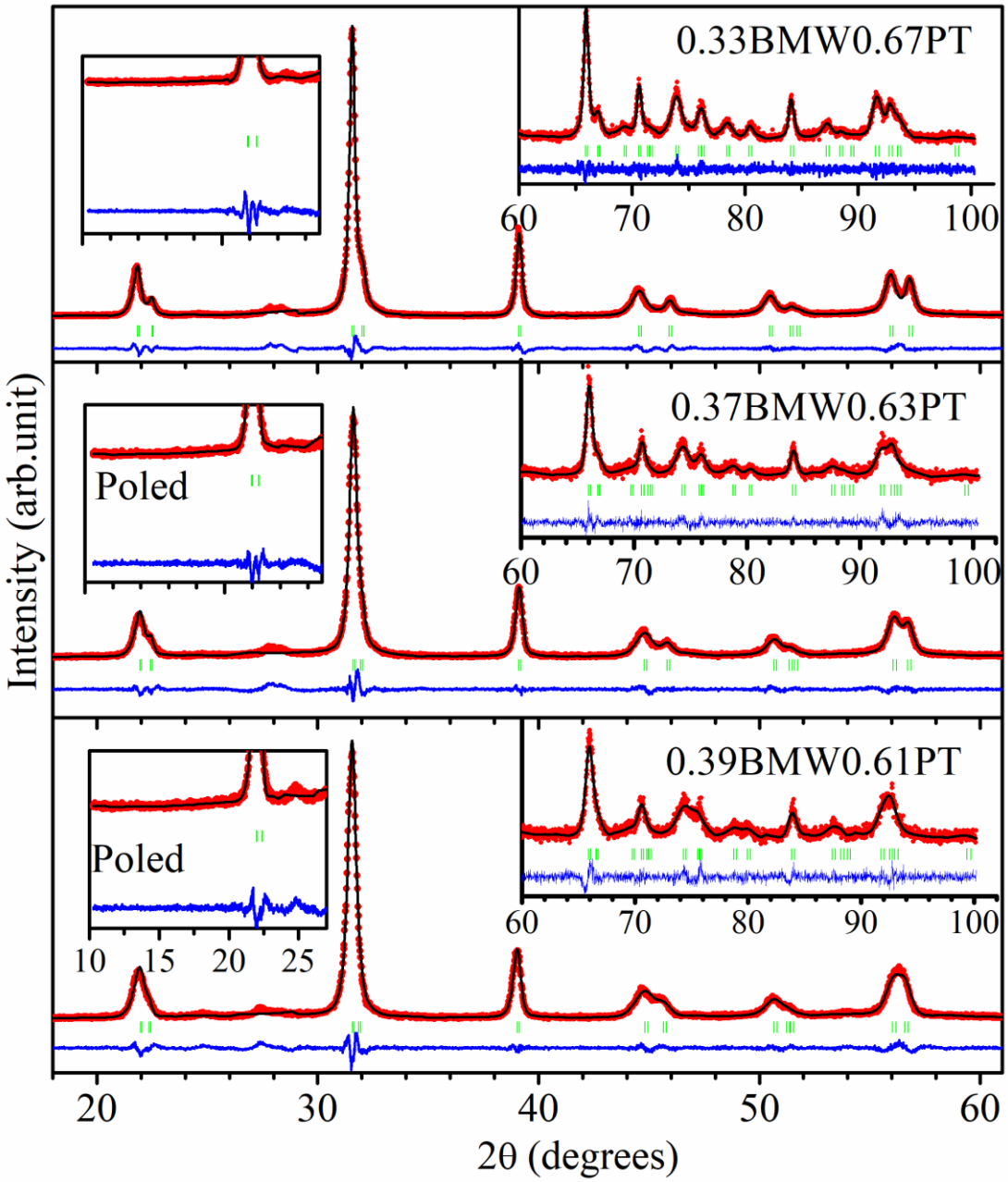

Figure 5.6 Experimentally Observed (red color dots), Rietveld calculated (continuous black line) and their difference (continuous bottom blue line) profiles obtained after full pattern Le-Bail profile matching analysis of the powder XRD data using *P*4*mm* space group for (1-x)BMW-xPT ceramics with compositions x = 0.61, 0.63 and 0.67 poled at 30 kV/cm. The vertical bars (green) above the difference plot show the Bragg peaks.

5.3.5 Effect of Electric Field Poling on the Lattice Parameters of (1-x)BMW-xPT Ceramic

Fig. 5.7 shows a comparison of lattice parameters for poled (30 kV/cm) and unpoled samples of (1-x)BMW-xPT ceramics with compositions x = 0.61, 0.62, 0.63 and 0.67. The lattice parameters for the unpoled and poled sample of (1-x)BMW-xPT are denoted by a_T, c_T, and a_{T_P}, c_{T_P}, respectively. As can be seen from **Fig. 5.6** the lattice parameters of the composition x = 0.67 remains unchanged after electric field poling possibly because of lower structural instability of this composition due to being away from the morphotropic phase boundary. Both the a- and c- parameters of the tetragonal phase for the compositions with x = 0.62 and 0.63 exhibit slight reduction after electric field poling. In contrast, the a- parameters of the tetragonal phase is slightly reduced while c- parameter is slightly enhanced after electric field poling for the compositions with x = 0.61. Such a variation of lattice parameter for lower composition might be due to larger coexistence of cubic phase in these compositions.

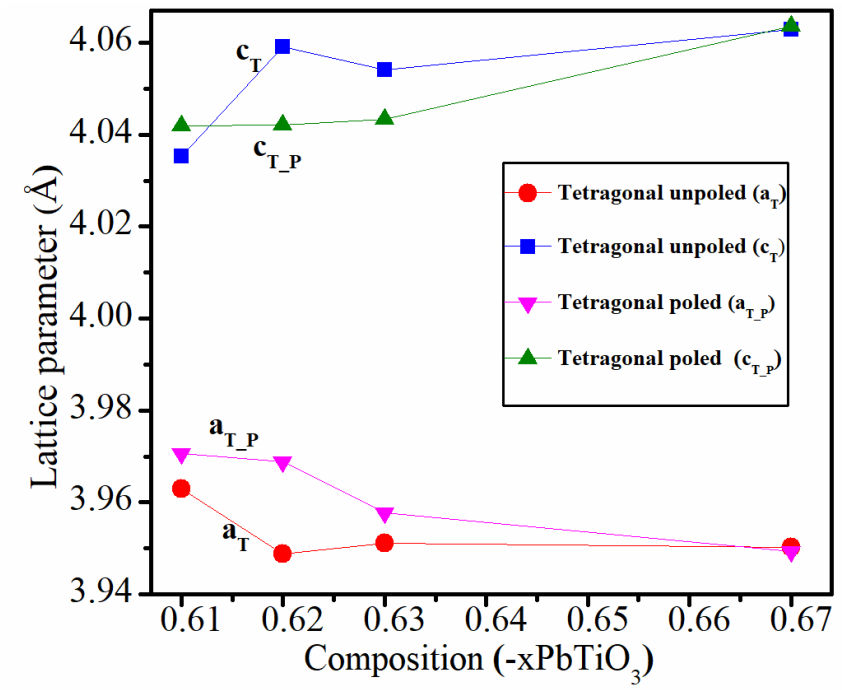

Figure 5.7 Comparison of lattice parameters for poled (30 kV/cm) and unpoled samples of (1-x)BMW-xPT ceramics with compositions x = 0.61, 0.62, 0.63 and 0.67.

The lattice parameters of unpoled and poled samples of (1-x)Bi($Mg_{3/4}W_{1/4}$)O_3-x$PbTiO_3$ ceramics for various field strengths are listed in **Table 5.1**. **Fig. 5.8** shows the poling field dependent variation of lattice parameters and unit cell volume of the tetragonal phase for 0.39BMW-0.61PT ceramic. Both the a- and c- lattice parameters and unit cell volume decrease linearly with increasing poling field strength. Reduction in the unit cell volume and lattice parameters with increasing field strength may be attributed to the structural transformation of the ordered (cubic, tetragonal) phases into disordered tetragonal (*P*4*mm*) phase. As shown in Chapter 3, composition dependence of the unit cell shows decreasing trend with increasing PT concentration. Apart from the ionic radii considerations, the appearance of disordered structure is also contributing to the decrease in the unit cell volume as the structural distortions at the local level will be smaller in this case. Inset to **Fig. 5.8** shows the c-axis lattice strain for different fields

for the tetragonal phase resulting due to electric field poling. The c- axis lattice strain was calculated using lattice parameter of poled and unpoled samples using following equation: Lattice strain (%) = [$C_{unpoled}$ - C_{poled}/C_{poled}] x 100. Strain level of ~0.51 % is obtained at the electric field strength of 50 kV/cm, which is quite significant.

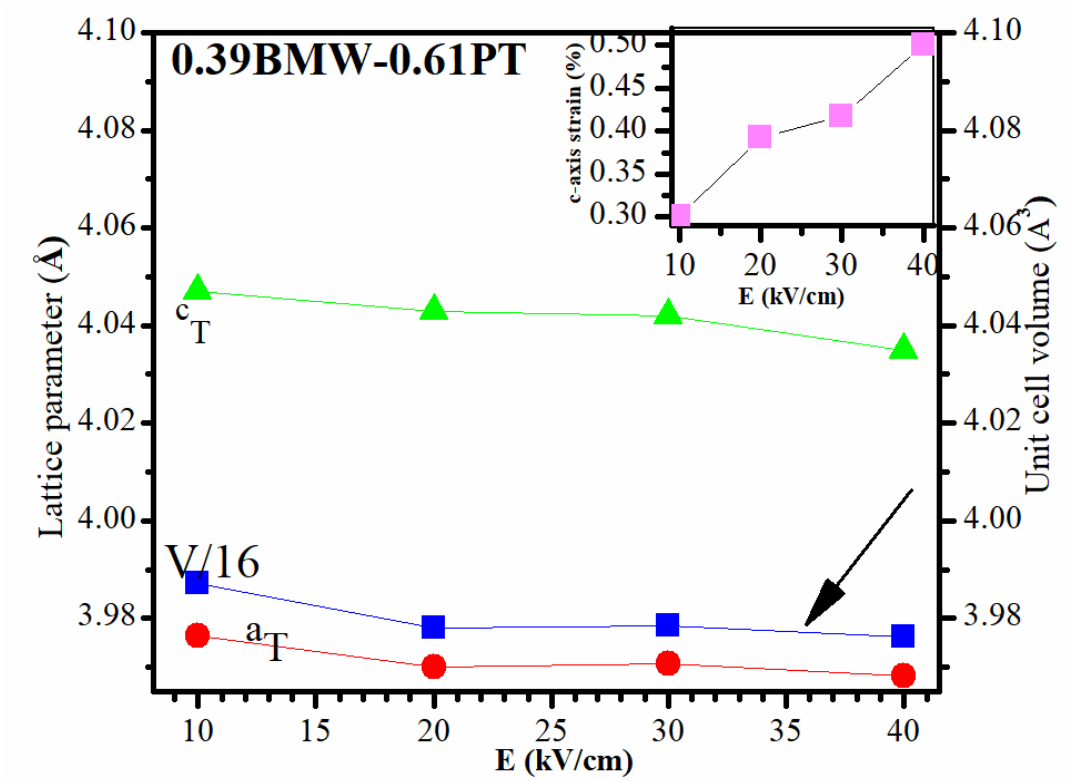

Figure 5.8 Poling field dependent variations of lattice parameters and unit cell volume of the tetragonal phase for 0.39BMW-0.61PT ceramic. Inset shows the c-axis lattice strain for different fields for the tetragonal phase.

Table 5.1: Lattice parameters of unpoled and poled samples of (1-x)Bi($Mg_{3/4}W_{1/4}$)O_3-x$PbTiO_3$ ceramics.

Compositions	Poling field (kV/cm)	Lattice parameters		
		(*Fm*-3*m*/*Pm*-3*m*) a = b = c	(*I*4/*m* or *P*4*mm*) a = b	(*I*4/*m* or *P*4*mm*) c
0.39BMW-0.61PT	0	7.99185(7)	5.66074(7)	7.91215(1)
	10		3.97646(5)	4.04500(2)
	20		3.97000(4)	4.04300(3)
	30		3.97064(4)	4.04200(1)
	40		3.96825(3)	4.0350(2)
0.37BMW-0.63PT	0	7.99325(9)	5.59526(3)	8.10403(6)
	10		3.95583(4)	4.04061(4)
	20		3.95706(3)	4.03824(4)
	30		3.95773(4)	4.04335(4)
	40		3.96443(6)	4.04707(1)
0.33BMW-0.67PT	0	7.64329(3)	5.58914(3)	8.12759(5)
	10	3.98399(2)	3.94702(2)	4.04714(1)
	20		3.94937(3)	4.06391(3)
	30		3.94938(1)	4.06365(1)

5.4 Conclusions

The crystal structure analysis of the electric field poled samples of (1-x)Bi($Mg_{3/4}W_{1/4}$)O_3-x$PbTiO_3$ ceramics reveals that the coexisting ordered cubic and ordered tetragonal phases close to the MPB compositions transform into disordered ferroelectric tetragonal phase with *P*4*mm* space group. The lattice parameters and unit cell volume slightly decrease after electric field poling due to the transformation from the ordered to disordered structure. The electric field induced structural transformation is associated with large c-axis lattice strain of 0.51% in the MPB composition.